

Electropulsing-induced phase transformations in a Zn–Al-based alloy

Yaohua Zhu,^{a)} Sandy To, and Wingbun Lee

Department of Industrial and Systems Engineering, The Hong Kong Polytechnic University, Hong Kong 852, China

Xingming Liu

Hefei National Laboratory for Physical Science at Microscales, University of Science and Technology of China, Hefei 230026, China

Yanbin Jiang and Guoyi Tang

Graduate School at ShenZhen, Tsinghua University, Tsinghua 518055, China

(Received 7 January 2009; accepted 15 April 2009)

Microstructural changes and phase transformations of an electropulsing-treated (EPT) ZA22 alloy wire were studied using scanning electron microscopy and transmission electron-microscopy techniques. Two stages of phase transformation were detected in the EPT alloy: (i) quenching from the as-furnace cooled (FC) state to the final stable state and (ii) up-quenching from the final stable state back to the as-FC state through two reverse phase transformations: $T' + \eta \rightarrow \alpha + \varepsilon$ and $\eta'_{T+\varepsilon+\alpha} \rightarrow \eta'_{FC}$. Electropulsing accelerated phase transformation tremendously. It was at least 1200 times faster than the aging process. The mechanism of the electropulsing-induced phase transformations is discussed from the point of view of Gibbs free energy and electropulsing kinetics.

I. INTRODUCTION

An electropulsing treatment (EPT) was found to be able to reduce residual stress in the 1960s.¹ As an alternative to the traditional thermal and mechanical processes, EPT has been recognized for its high efficiency, and extensive studies in materials science and engineering have been carried out in such areas as electroplasticity,^{2–4} electromigration,^{5,6} recrystallization,^{7–9} phase transformations,^{10–15} and in the mechanism of interaction between electrons and lattice atoms and dislocation movement.^{16–18} EPT has also been applied to materials processing, in such areas as cold drawing, recovering cracks and flaws, and refining grain size, as well as in biology and environmental protection and in the medical domain.^{19–23}

Previous studies indicated that EPT enhanced rates of both crystallization and recrystallization of alloys.^{7,9} Compared with the conventional processes, microstructure and grain size were remarkably refined, and the material properties were improved. It was recently reported that, with adequate electropulsing, the elongation of the Zn–Al-based alloy was increased by 437% at ambient temperature under high strain rate, whereas the instantaneous tensile stress remained unchanged compared with that of the non-EPT alloy.¹⁴ This was significant from a practical point of view.

However, little has been studied on the effects of electropulsing on the microstructural evolution and phase transformations of alloy materials. As one of the driving forces for phase transformation and processing, electropulsing is more powerful and more effective than thermal energy. Traditional thermodynamics are not sufficient to explain electropulsing behaviors. It is of important theoretical significance to explore the mechanism of EPT processing.

Thus, this work was initiated to study the effect of electropulsing on microstructural changes and phase transformations in a furnace-cooled (FC) Zn–Al-based alloy wire, based on systematic studies of the alloys.^{24–32}

II. EXPERIMENTAL PROCEDURES

An ingot of an eutectoid Zn–Al-based alloy ZnAl22Cu2.2 (in wt%) was repeatedly extruded at 250 °C to produce gross wire of 9.5 mm in diameter. After being cold drawn and repeatedly tempered at 250 °C, an alloy wire of 1.5 mm in diameter was produced. Samples of this wire specimen were solution treated at 350 °C for 4 days and cooled inside the furnace chamber, i.e., FC to ambient temperature. The heat-treated alloy wire was cut into pieces 100 mm in length for EPT. A self-made electropulsing generator was applied to discharge positive direction multiple pulses with a current intensity of 10 A. The frequency of the multiple electropulses was selected as 100 Hz. The duration of each pulse was kept to ~2300 μs. Using an oscilloscope with a Hall effect component, the peak current density J_m and the

^{a)}Address all correspondence to this author.

e-mail: yaohuazhu@hotmail.com

DOI: 10.1557/JMR.2009.0300

root-mean-square (RMS) value of current density J_e were determined as 8.1269 A and 1.8518 A/mm², respectively. A jet oil cooling system was used to cool and protect the surface of the wire specimens. The surface temperature of the specimens, measured with a thermocouple, was 28 °C. Duplicate wire specimens were electropulsing treated for 10, 30, and 60 s.

Longitudinal cross-sections of both non-EPT and EPT wire specimens were polished and examined using scanning microscopy in the backscattered electron mode (BSEM) to produce a medium resolution of atomic contrast among the various phases involved. Also, examination of conventional transmission electron microscopy (TEM) was carried out using a JEOL 2010 transmission electron microscope. Thin foil specimens were produced using ion-beam milling.

III. RESULTS AND DISCUSSION

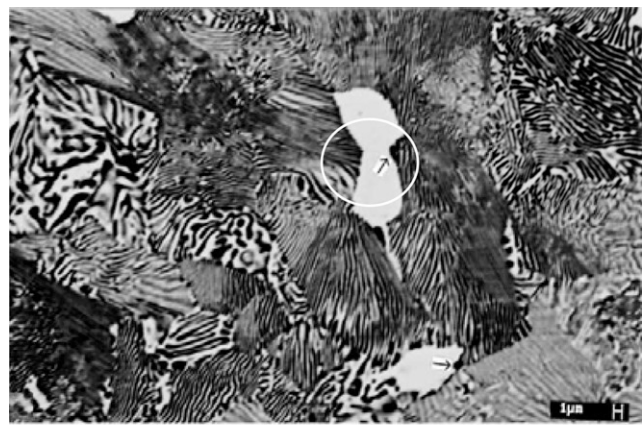
A. Phase transformations in the FC ZA22 alloy during aging

Decomposition of the supersaturated phases in the FC alloys consisting of two steps of phase transformation occurred during the thermal or thermo-mechanical processes.^{27,28}

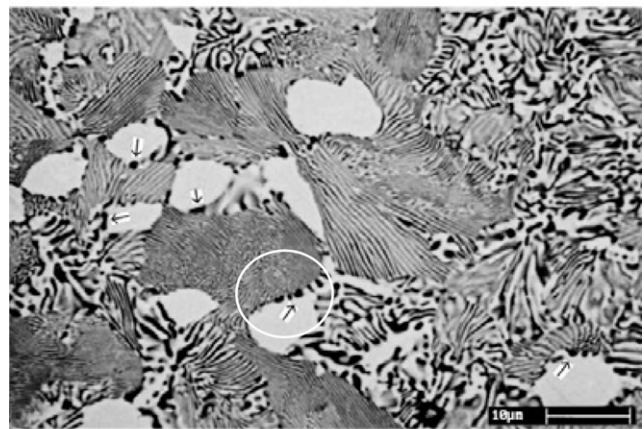
1. Decomposition of η'_{FC} phase: $\eta'_{FC} \rightarrow \eta'_T + \alpha + \varepsilon$

On BSEM observation,²⁶ precipitation of the α phase inside the η phase is one of the characteristics of the decomposition of the η'_{FC} phase (Zn-rich phase of hcp structure) in the FC ZA alloy. Dark-imaged α phase precipitates (Al-rich phase of fcc structure) were developed inside the light-imaged η phase during the early stage of aging. The ε phase was an hcp compound Zn₄Cu. Shown in Fig. 1 is the evolution of the α phase precipitation during aging at 100 °C. A small amount of the dark-imaged α phase precipitates was observed at the grain boundaries of the η phase, as indicated by an arrow in Fig. 1(a). After 30 h of aging at 100 °C, α phase precipitates developed more generally, as shown in Fig. 1(b).

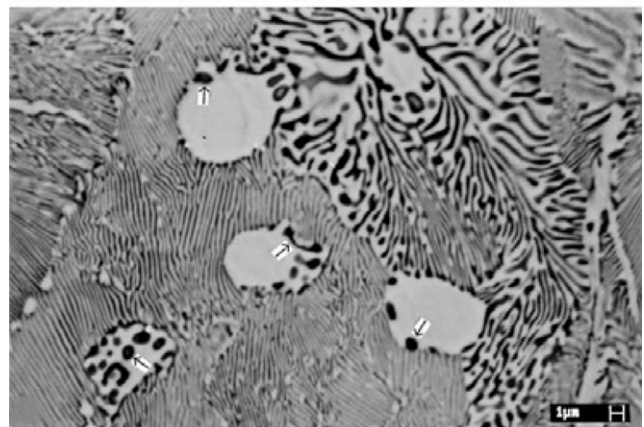
From the x-ray diffraction (XRD) examination using nickel-filtered Cu K_α radiation,^{26,27} it was observed that the (0002) diffraction at 36.8° in the FC ZA specimen decreased in intensity, whereas a metastable η'_T phase appeared at a lower 2θ : 36.5°. The calculated d-spacings of the η'_{FC} phase and the η'_T phase were 0.2437 and 0.2456 nm, respectively. The c/a value of the η'_{FC} phase increased during its decomposition. Meanwhile, the diffraction lines of the α phase and the ε phase increased in intensity. The decomposition of the η'_{FC} phase occurred during aging as a discontinuous precipitation: $\eta'_{FC} \rightarrow \eta'_T + \alpha + \varepsilon$. This was co-related to a known phases equilibrium, $\beta + \varepsilon \rightarrow \eta + \alpha$, at 276 °C.^{24,25}



(a)



(b)



(c)

FIG. 1. BSEM images of as-FC and 100 °C-aged ZA 22 specimen: (a) as-FC state, (b) 100 °C aged for 10 h, and (c) 100 °C aged for 30 h.

2. Four-phase transformation: $\alpha + \varepsilon \rightarrow T' + \eta$

On prolonged aging, a four-phase transformation occurred: $\alpha + \varepsilon \rightarrow T' + \eta$. The gray imaged T' phase precipitates increased in the light-imaged ε phase, confirming that the four-phase transformation was occurring. This was co-related to another phase equilibrium, $\alpha + \varepsilon = T' + \eta$, at 268 °C.^{24–27}

The above-mentioned two steps of the phase transformation were observed in various thermal or thermal-mechanical processes in the eutectoid FC ZA alloy.^{25,27,28}

B. Phase transformations in the EPT FC alloy

The microstructure of the FC alloy wire specimen was examined using BSEM. The FC alloy wire specimen consisted of coarse and fine lamellae and the light-imaged η'_{FC} and ε particles, as shown in Fig. 2(a). A small amount of the dark-imaged particles of precipitates of the α phase were observed at phase boundaries of the light-imaged η'_{FC} phase, as indicated by circles in Figs. 1(a) and 2(a).

A TEM bright-field image of the as-FC alloy specimen is shown in Fig. 3(a). Together with the indexed diffraction patterns, the dark-field images reflected from $[\bar{1}543] (\bar{2}11\bar{1})$ of the η'_{FC} phase, $[\bar{1}2\bar{1}3] (\bar{1}10\bar{1})$ of the ε phase, and $[\bar{1}12] (1\bar{1}\bar{1})$ of the α phase are shown in Figs. 3(b)–3(d). Using these selected area diffraction patterns (SADPs), the lattice parameters of the phases were determined as follows: η'_{FC} phase, $a = 2.735 \text{ \AA}$, $c = 4.871 \text{ \AA}$, and $c/a = 1.781$; ε phase, $a = 2.832 \text{ \AA}$, $c = 4.297 \text{ \AA}$ and $c/a = 1.517$; α phase, $a = 4.072 \text{ \AA}$.

In the case of EPT, the above-mentioned phase transformations were sped up tremendously. The BSEM image of the 10 A/10 s EPT specimen is shown in Fig. 2(b). In addition to the dark-imaged α phase precipitates, a large amount of the gray-imaged T' precipitates was observed,

as indicated by the arrows in Fig. 2(b). This implies that the phase transformation, $\alpha + \varepsilon \rightarrow T' + \eta$, was terminated after 10 A EPT for 10 s. TEM examination confirmed the BSEM results. Shown in Fig. 4 is the bright field of the 10 A/10 s EPT specimen together with the diffraction pattern of the dark-imaged η_F phase in the specimen. No ε phase precipitates were observed in the phase lamellae. According to the previous study, this is the typical morphology of the final stable phase, shown in Fig. 5(a).¹⁴ It was also observed that ε phase precipitation increased as current intensity increased in the reverse phase transformation, $T' + \eta \rightarrow \alpha + \varepsilon$, as shown in Fig. 5. Both BSEM and TEM examinations ascertained that the specimen reached the final stable state after 10 A EPT for 10 s.

After EPT for 30 s, the gray precipitates of the T' phase disappeared. The dark-imaged α phase precipitate increased inside the light-imaged η'_{FC} phase, as marked by a circle in Fig. 2(c). The BSEM image of the 10 A/30 s EPT specimen was similar to that of the 100 °C /10 h aged FC alloy specimen. The latter is shown in Fig. 1(b). The similar morphologies are marked by circles in Figs. 2(c) and 1(b). From this comparison, it can be seen that both BSEM morphologies of the precipitates of the α phase in the η'_{FC} phase are similar. This implied that, after EPT for 30 s, the specimen had up-quenched from the final stable state back to the 100 °C /10 h aged state of the alloy specimen.

A detailed microstructural examination of the 10 A/30 s EPT specimen was carried by TEM. The TEM bright-field

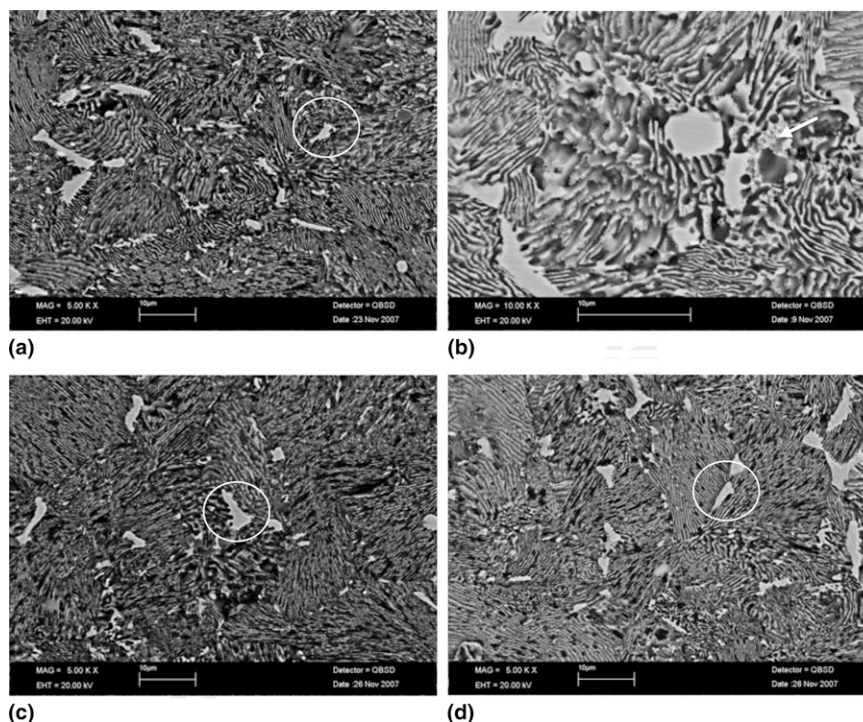


FIG. 2. BSEM images of (a) ZA22 non-EPT and (b) 10 s EPT, (c) 30 s EPT, and (d) 60 s EPT FC specimen, showing quenching [from (a) to (b)] and up-quenching [from (b) to (d)] processes.

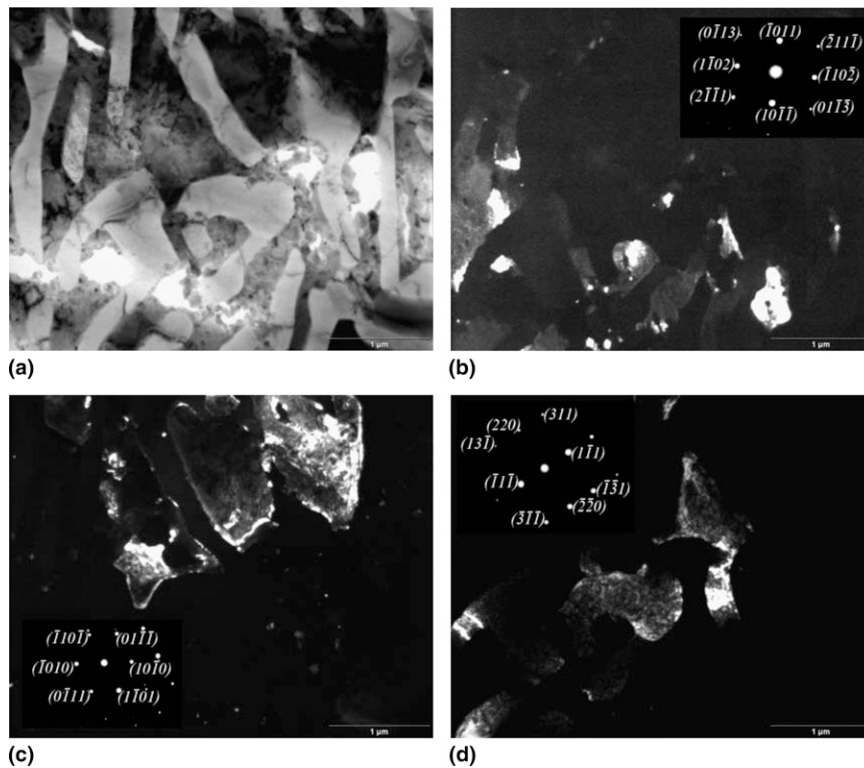


FIG. 3. (a) TEM bright image, (b) dark-field image of $(\bar{2}11\bar{1})$ reflection together with diffraction pattern from $B = [\bar{1}5\bar{4}3]$ of the η'_{FC} phase, (c) dark-field image of $(\bar{1}2\bar{1}3)$ reflection together with diffraction pattern from $B = [\bar{1}2\bar{1}3]$ of the ϵ phase, and dark-field image of $(1\bar{1}1)$ reflection together with diffraction pattern from $B = [\bar{1}12]$ of the α phase of the as-FC ZA22 alloy specimen.

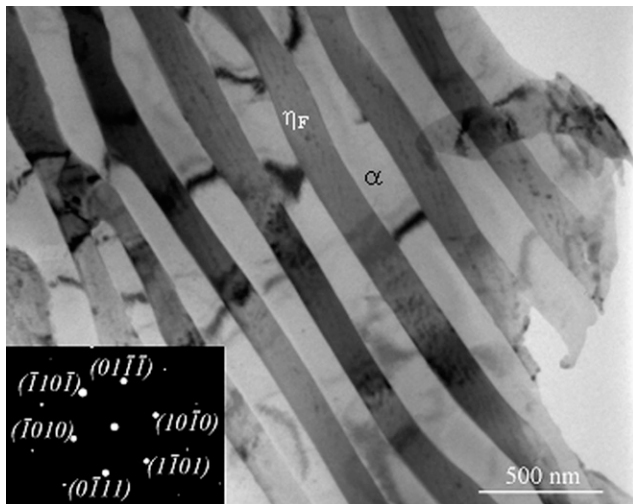


FIG. 4. Bright-field image and the diffraction pattern of the dark-field imaged η_F phase of the 10 A/10 s EPT ZA22 alloy specimen.

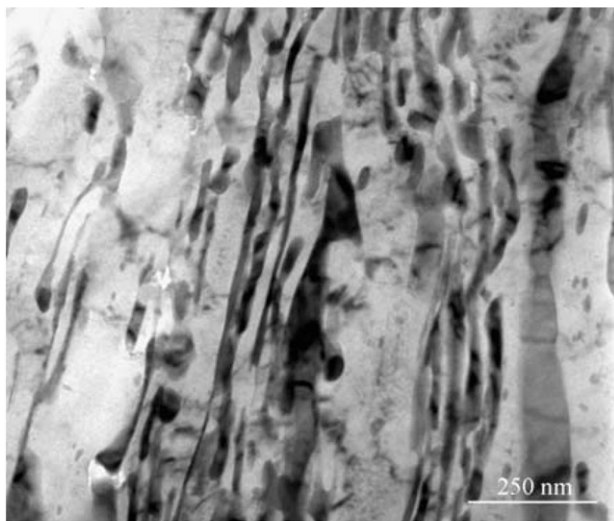
image of this specimen is shown in Fig. 6(a). Together with the indexed diffraction patterns, the dark-field images reflected from $[\bar{1}5\bar{4}3]$ $(1\bar{1}02)$ of the η'_{FC} phase, $[\bar{1}100]$ $(\bar{1}\bar{1}20)$ of the η'_T phase, $[2\bar{1}\bar{1}0]$ (0110) of the ϵ phase, and $[\bar{1}12]$ (131) of the α phase are shown in Figs. 6(b)–6(e), respectively. Using these SADPs,

the lattice parameters of the phases were determined as follows: η'_{FC} phase, $a = 2.707 \text{ \AA}$, $c = 4.924 \text{ \AA}$ and $c/a = 1.818$; η'_T phase, $a = 2.694 \text{ \AA}$, $c = 4.950 \text{ \AA}$ and $c/a = 1.837$; ϵ phase, $a = 2.733 \text{ \AA}$, $c = 4.261 \text{ \AA}$ and $c/a = 1.559$; α phase, $a = 4.072 \text{ \AA}$ respectively. Four phases, η'_{FC} , η'_T , ϵ , and α , appeared to coexist adjacent to each other.

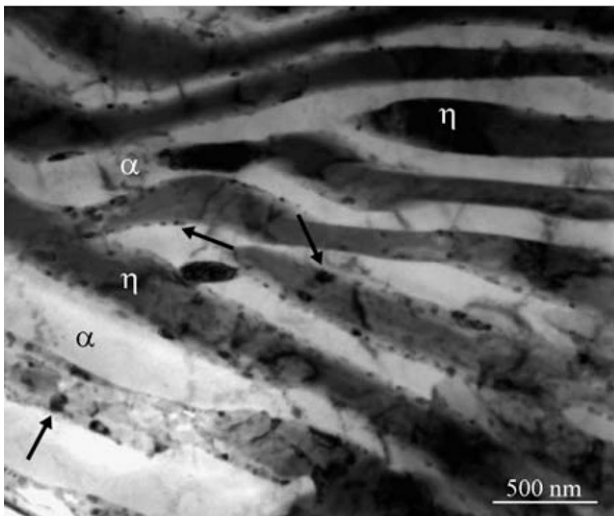
From both BSEM and TEM results, it was shown that, during electropulsing from 10 to 30 s, the T' phase disappeared through reverse phase transformation, $T' + \eta \rightarrow \alpha + \epsilon$, and another reverse phase transformation, $\eta'_T + \epsilon + \alpha \rightarrow \eta'_{FC}$, had occurred.

After EPT for 60 s, the precipitates of the α phase inside the light-imaged η'_{FC} phase decreased, as shown in Fig. 7. The BSEM image of the 10 A/60 s EPT specimen was very similar with that of the as-FC alloy specimen, as indicated by circles in Figs. 2(d) and 1(a). The TEM bright-field image together with the indexed $[2\bar{1}\bar{1}0]$ diffraction pattern is shown in Fig. 7.

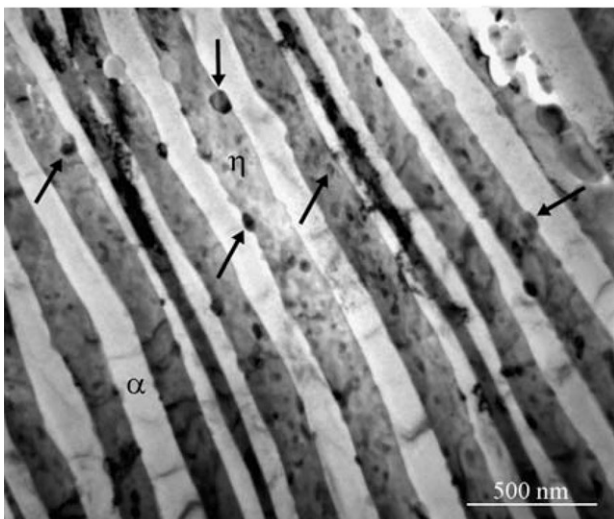
The lattice parameters of the phases were determined as follows: η'_{FC} phase, $a = 2.733 \text{ \AA}$, $c = 4.950 \text{ \AA}$ and $c/a = 1.811$; α phase, $a = 4.064 \text{ \AA}$. From both BSEM and TEM examinations, it was ascertained that the reverse transformation, $\eta'_T + \epsilon + \alpha \rightarrow \eta'_{FC}$, was completed, and the alloy specimen recovered back to the FC state after 10 A/60 s EPT.



(a)



(b)



(c)

FIG. 5. TEM bright-field images of the neck zones of the (a) 15, (b) 20, and (c) 30 A EPT specimens, showing the ϵ phase precipitates increased with increasing current intensity from 15 to 30 A.

Compared with the BSEM and XRD results of the aged FC alloy specimens,^{27,28} the evolution of the lattice parameters of the phases η'_{FC} , η'_T , and η_F in the EPT alloy specimens confirms the above-mentioned phase transformation, $\alpha + \epsilon \rightarrow T' + \eta$, and two reverse phase transformations, $T' + \eta \rightarrow \alpha + \epsilon$ and $\eta'_T + \epsilon + \alpha \rightarrow \eta'_{FC}$. The lattice parameters of the zinc rich phases, η'_{FC} , η'_T , and η_F , in the EPT alloy specimens are listed in Table I.

In previous studies, it was found that the decomposition of the η'_{FC} phase was characteristic of the shifting of the x-ray diffraction peak to a lower 2θ angle, whereas the c axis and c/a increased.^{24–32} In Table I, it is clearly seen that c/a (η'_{FC}) $<$ c/a (η'_T) $<$ c/a (η_F). These stages are indicated by two arrows in Table I:

(a) Phase transformations in a way of quenching: in the first 10 s of 10 A EPT, i.e., transformation from the as-FC state to the final state, through $\eta'_{FC} \rightarrow \eta'_T + \alpha + \epsilon$ and $\alpha + \epsilon \rightarrow T' + \eta$, the c/a (η'_{FC}) 1.781 increased to c/a (η_F) 1.900.

(b) Reverse phase transformations in the way of up-quenching: during 10–30 s of 10 A EPT, transformation from the final stable state to the 100 °C / 10 h aged state occurred. The T' phase disappeared by reverse phase transformation, $T' + \eta \rightarrow \alpha + \epsilon$, and another reverse phase transformation, $\eta'_T + \epsilon + \alpha \rightarrow \eta'_{FC}$, occurred. The four phases, η'_T , ϵ , α' and η'_{FC} , were examined, and the c/a (η_F) 1.900 decreased to c/a (η'_T) 1.873, and c/a (η'_{FC}) being back to 1.818. During 30–60 s of 10 A EPT, a reverse transformation from the 100 °C / 10 h aged state back to the as-FC state occurred as $\eta'_T + \epsilon + \alpha \rightarrow \eta'_{FC}$. The η'_T vanished, and the c/a (η'_{FC}) reversed to 1.811.

The above-mentioned correlation between the phase transformations in the aged and EPT alloys is schematically shown in Fig. 8, where the quenching process of 10 s is represented by a bold solid line and the up-quenching process of 50 s is indicated by a dashed bold line on the 10 A EPT duration axis. It is evident that the early stage of the EPT-induced reverse phase transformation is related with the prolonged stage of phase transformation during aging, whereas the reverse phase transformations that occurred during the prolonged stage of the EPT correspond to that observed in the early stage of aging.

It is surprising to notice that, under 10 A EPT, the above-detected two stages of phase transformation took only 60 s at ambient temperature (28 °C). The first stage took only 10 s. In comparison with the non-EPT processes, the four-phase transformation, $\alpha + \epsilon \rightarrow T' + \eta$, occurred after aging at 170 °C for 52 h, and it took at least 12 min in the 100 °C tensile deformation.

Although the duration of the second stage, i.e., the two reverse phase transformations, was 50 s, the reverse transformation, $\eta'_T + \epsilon + \alpha \rightarrow \eta'_{FC}$, was detected after only

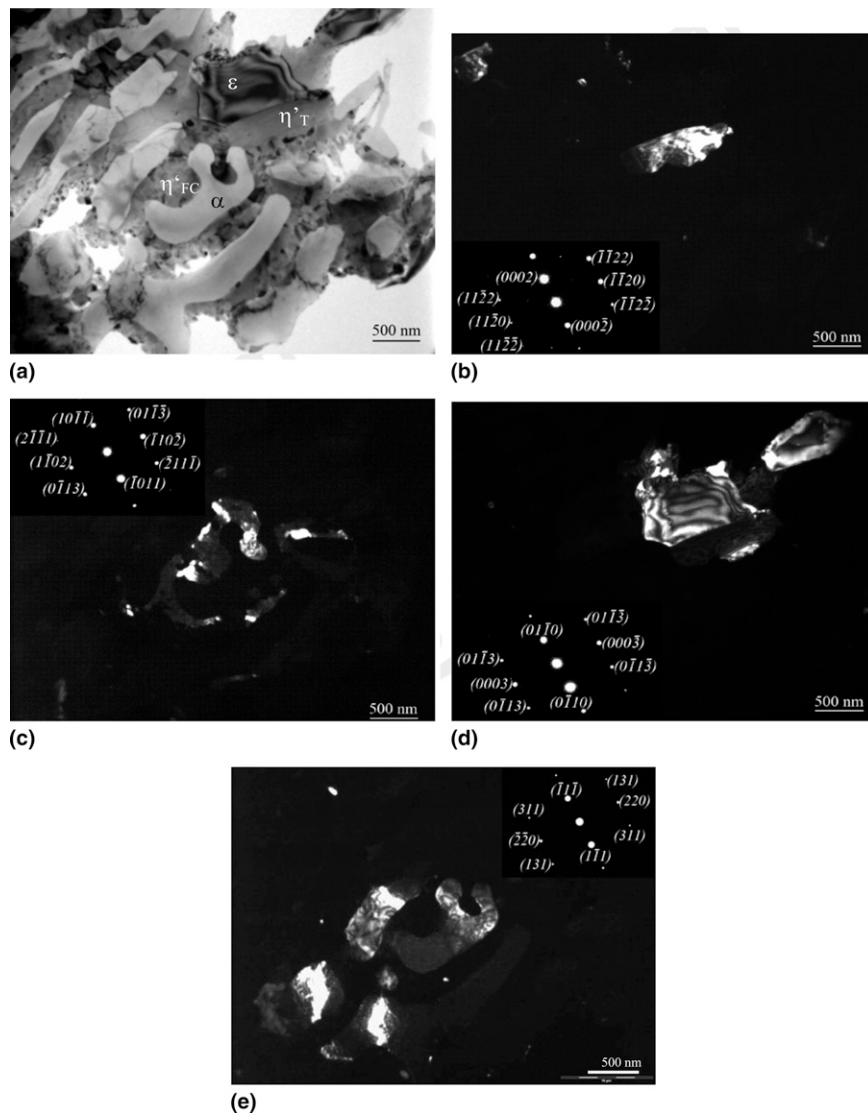


FIG. 6. (a) TEM bright image, (b) dark-field image of $(\bar{1}\bar{1}02)$ reflection together with diffraction pattern from $B = [\bar{1}\bar{1}\bar{5}43]$ of the η'_T phase, (c) dark-field image of $(\bar{1}\bar{1}20)$ reflection together with diffraction pattern from $B = [\bar{1}\bar{1}00]$ of the η'_{FC} phase, (d) dark-field image of $(0\bar{1}10)$ reflection together with diffraction pattern from $B = [2\bar{1}\bar{1}0]$ of the ϵ phase, and (e) dark-field image of (131) reflection together with diffraction pattern from $B = [\bar{1}\bar{1}2]$ of the α phase of the 10 A/30 s EPT ZA22 alloy specimen.

30 s of 10 A EPT at ambient temperature (28 °C). In the case of aging, it took 10 h of aging at 100 °C to detect $\eta'_{FC} \rightarrow \eta'_T + \alpha + \epsilon$. Under electropulsing, the phase transformation was accelerated at least by 1200 times, because the effect of temperature on the phase transformation had not yet been under consideration.

Obviously, the electropulsing tremendously accelerates phase transformations in both quenching and up-quenching in the Zn–Al-based alloy compared with the aging process.

It should be pointed out that the reverse phase transformations, $T' + \eta \rightarrow \alpha + \epsilon$ and $\eta'_T + \epsilon + \alpha \rightarrow \eta'_{FC}$, have never been observed in any thermal or thermo-mechanical processes (e.g., aging, tensile, creep, fatigue, and damping).^{25–32}

C. Driving force for the EPT-induced phase transformations

The driving force for phase decomposition consists of various parts: chemical Gibbs free energy, surface energy, strain energy, the Gibbs free energy induced by crystal orientation, the electropulsing-induced Gibbs free energy, and so on, as follows:

$$\Delta G = \Delta G_{\text{chem}} + \Delta G_{\text{stress}} + \Delta G_{\text{surf}} + \Delta G_{\text{orient}} + \Delta G_{\text{ep}} \dots$$

The chemical Gibbs free energy, ΔG_{chem} , is considered as a main part of the driving force as far as thermodynamics are concerned. The strain energy, ΔG_{stress} , includes various internal strain energies that may be available, e.g., because of thermal stress during

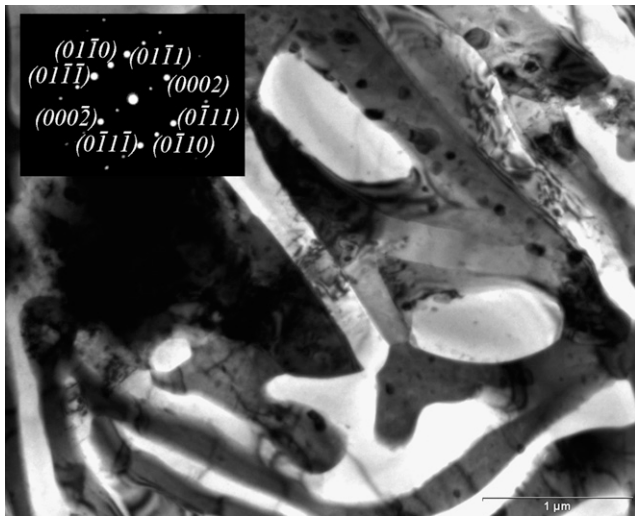


FIG. 7. Bright-field image and the indexed diffraction pattern [2110] of the dark-imaged η'_{FC} phase of the 10 A/60 s EPT ZA22 alloy specimen.

TABLE I. Lattice parameters of the zinc-rich phases: η'_{FC} , η'_T , and η_F at various stages of EPT.

States	c/a (η'_{FC})	$<$	c/a (η'_T)	$<$	c/a (η_F)
as-FC	1.781				
10 A EPT for 10 s		(a)			1.900
10 A EPT for 30 s	1.818	(b)	1.873		
10 A EPT for 60 s	1.811				

^aPhase transformations in a way of quenching from the as-FC state to the final stable state.

^bReverse phase transformations in a way of up-quenching from the final stable state to the FC state.

solidification of melt, and external strain energies (because of tensile, creep, fatigue, damping, and milling deformations, etc.).^{24–32} In dealing with the decomposition of the nanophases in the films of the Zn–Al-based alloys, the surface energy, ΔG_{surf} , and the preferred crystal orientation induced Gibbs free energy, ΔG_{orient} , become dominant factors in affecting the phase transformations.³²

The electropulsing tremendously accelerated the phase transformations in two stages:

(i) When $\Delta G < 0$, with addition of electropulsing-induced Gibbs free energy, ΔG_{ep} , the total Gibbs free energy of the as-FC alloy was increased and was much higher than that of the final stable alloy. The driving force for the phase transformation was significantly increased. The electropulsing accelerates decomposition of the supersaturated phases from the supersaturated state of the as-FC alloy specimens approaching the saturated state, i.e., final stable state, where $\Delta G = 0$. The BSEM and TEM examinations confirmed that the final state of the alloy was reached after 10 s of 10 A EPT.

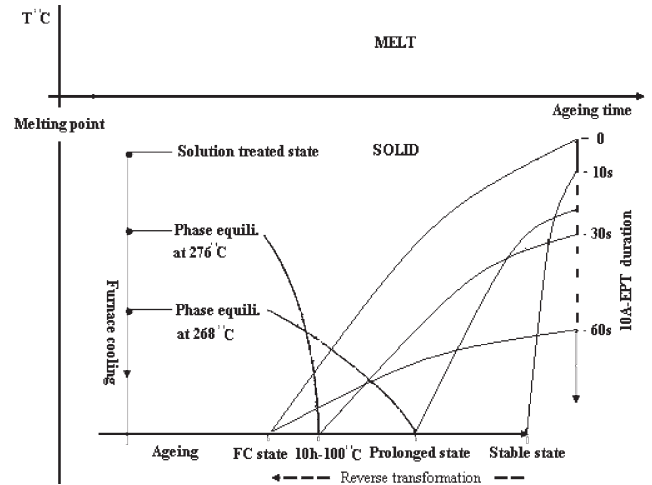


FIG. 8. Correlation between phase transformations in the aged and EPT alloys, showing a quenching process from the FC state to the final stable state in the first 10 s of EPT (bold solid line) and the up-quenching process from stable state back to the FC state (the reverse phase transformations) in the subsequent 50 s of EPT (dashed bold line).

(ii) When $\Delta G = 0$, further electropulsing increased the Gibbs free energy of the alloy to above that of the final stable state. ΔG became positive, i.e., $\Delta G > 0$; the saturated phases, i.e., the stable phases, reverse-decomposed. Two kinds of reverse phase decomposition occurred, $T' + \eta \rightarrow \alpha + \varepsilon$ and $\eta'_T + \varepsilon + \alpha \rightarrow \eta'_{FC}$, in the second stage of phase transformation. After 10 A EPT for 50 s, the alloy reverse-transformed back to the as-FC state in the second stage.

In our recent study,^{14,15} the reverse four-phase transformation, $T' + \eta \rightarrow \alpha + \varepsilon$, was detected in the dynamic EPT ZA alloy, which was co-related to the equilibrium, $\alpha + \varepsilon = T' + \eta$, at 268 °C.^{27,28} However, the reverse phase transformation, $\eta'_T + \varepsilon + \alpha \rightarrow \eta'_{FC}$, was detected for the first time in the EPT alloy specimens. The newly detected reverse phase transformation, $\eta'_T + \varepsilon + \alpha \rightarrow \eta'_{FC}$, was co-related to the equilibrium, $\beta + \varepsilon = \eta + \alpha'$ at 276 °C.²⁴ This implies that, if the EPT provides a sufficient increment of Gibbs energy, the solid state at an even higher temperature could be reached.

It is interesting to notice that the quenching process, i.e., the phase decomposition from the as-FC state to the final state, was completed in 10 s, whereas the up-quenching process, i.e., that from the final stable state back to the as-FC state, took 50 s. In other words, under 10 A EPT, the phase transformations in the quenching process were faster than the reverse phase transformations in the up-quenching process by five times and at least by 6000 times (i.e., 1200×5) compared with that in the non-EPT quenching process.

For the quenching process, both ΔG_{chem} and ΔG_{ep} are negative: then, $|\Delta G_{quen}| = -|\Delta G_{chem}| - |\Delta G_{ep}|$. In the

case of the up-quenching process, the driving force ($\Delta G_{\text{up-quench}}$) is only from the increment of the Gibbs free energy because of electropulsing, ΔG_{ep} . Because of the positive increment of ΔG_{ep} , the EPT alloy specimen becomes unstable and reverse-transforms back to the original FC state.

Moreover, once the alloy leaves from the stable state at the EPT operating temperature (28 °C) and is up-quenched to a higher temperature, the ΔG_{chem} becomes negative again. The positive $|\Delta G_{\text{up-quench}}| = -|\Delta G_{\text{chem}}| + |\Delta G_{\text{ep}}|$ is reduced. Therefore, $|\Delta G_{\text{quench}}| > |\Delta G_{\text{up-quench}}|$, and the driving force for the up-quenching process is smaller than that for the quenching process. It takes a longer time to complete the reverse phase transformation.

D. Electropulsing kinetics

Previous studies indicated that, under electropulsing, the electron wind formed by the knock-on collision of high-rate electrons with atomic nuclei was beneficial to the mobility of dislocation.^{2,7,17} Under the impact of transient stress, mobilized dislocations were moving very quickly, even at ultrasonic speeds.¹⁷ The transfer of energy from the electrons directly to the atoms was much more effective than that in the traditional thermal and thermo-mechanical processes. From the point of view of thermodynamics, a process with a high rate of increase in supersaturation, i.e., the driving force for phase transformations, is called “quenching.” EPT is also a kind of quenching process, called “electropulsing-quench” or “ep-quench,” being distinct from “water-quench,” which is used in heat treatment.

It was supposed that the electropulsing effectively affected the sliding behavior of the dislocation and the activity of vacancies.¹⁶ As far as the diffusion-controlled phase transformations are concerned, it is anticipated that electron migration may be important when considering the influence of an electric current. The effect of the atomic diffusion flux, J , on both precipitation rate and on the motion of quench-in vacancies and dislocation to the grain boundaries and sinks is important.

The effect of electric current on the atomic drift flux of atoms in metals is given by the Nernst-Einstein equation.

$$J_i = \frac{N_i \cdot D_i}{KT} \left(KT \cdot \frac{\partial \ln X_i}{\partial x} - \Omega \cdot \frac{\partial \sigma}{\partial x} + Z^* \cdot e \cdot \rho \cdot j \right), \quad (1)$$

where N_i is the density of the i th atom species, D_i is the pertinent diffusion coefficient, Z^* is an effective valence, e the charge on an electron, ρ is the resistivity, j is the current density, X_i is the concentration of the i th solute, Ω atom volume, $-\frac{\partial \sigma}{\partial x}$ is the stress gradient, K is the Boltzmann constant, and T is the absolute temperature.

The effects of chemical potential gradient and composition gradient mentioned in Eq. (1) were neglected here

because these effects were much weaker than that of electropulsing. In the case of electropulsing, the J consists of two parts, J_t and J_a , where J_t is the flux of diffusion atoms caused by the thermal effect, and J_a is the flux of the diffusion atoms because of the athermal effect.^{21–23}

The average atomic flux per second during multiple continuous electropulsing can be derived from Eq. (1) and described by Eq. (2).⁹

$$J = J_t + J_a = \frac{2\pi D_l}{\Omega \ln \left(\frac{R'}{\gamma_0} \right)} \cdot \left(1 + \frac{\delta c}{c_0} \right) + \frac{2N \times D_l \times Z^* \times e \times \rho \times f \times j_m \times \tau_p}{\pi KT}, \quad (2)$$

where D_l is the lattice diffusion coefficient, and N is the density of atom. The additional symbol c_0 is the average concentration of vacancy, δc is supersaturation concentration of vacancies, r_o and R' are the distances far from dislocation where the vacancy concentrations are c_0 and $c_0 + \delta c$, respectively; T is the absolute temperature; j_m , f , and τ_p are peak current density, frequency, and duration of each electropulse, respectively.

In this study, the electropulsing was performed at approximately ambient temperature. The J_t is small and neglected. The atomic flux for the total duration of EPT is written as Eq. (3):

$$J = J_a = \frac{2N \times D_l \times Z^* \times e \times \rho \times f \times j_m \times \tau_p \times t_{ept}}{\pi KT}. \quad (3)$$

Equation (3) thus shows that J_a is strongly dependent on the parameters of electropulsing and increases strongly with the peak current density, frequency f , duration of each electropulse τ_p , peak current density j_m , and the duration of EPT t_{ept} , when temperature T is constant.

Therefore, under electropulsing, a high peak current density and a longer duration t_{ept} are sufficient to accelerate dramatically the diffusional phase transformation at relatively low temperature in a very short period of time.

IV. CONCLUSIONS

(1) Electropulsing-induced phase transformations in the FC ZA22 alloy consist of two stages: (i) quenching from the FC state to the final stable state and (ii) up-quenching from the final stable state back to the as-FC state through two reverse phase transformations; consequently, $T' + \eta \rightarrow \alpha + \varepsilon$ and $\eta'_{T+\varepsilon+\alpha} \rightarrow \eta'_{\text{FC}}$.

(2) The early stage of the EPT-induced reverse phase transformation is related to the prolonged stage of phase transformation during aging, whereas the reverse phase transformations that occurred during the prolonged stage of the EPT correspond to those observed in the early stage of aging.

(3) Compared with the aging process, the EPT accelerates the reverse phase transformations in the Zn–Al-based alloy by a factor of at least 1200.

(4) Under electropulsing, the phase transformations in the quenching process are faster than the reverse phase transformations in the up-quenching process by a factor of 5 and are accelerated by a factor of at least 6000 compared with that in the aging process.

ACKNOWLEDGMENTS

The authors thank the Research Committee of the Hong Kong Polytechnic University for its financial support and J.M.N. Yueng and Ka Chun Chung for assistance in the experimental and editorial work.

REFERENCES

- O.A. Troitskii: Electromechanical effect in metals. *Zh. Eksp. Teor. Fiz.* **10**, 18 (1969).
- A.F. Sprecher, S.L. Mamna, and H. Conrad: On the mechanisms for the electroplastic effect in metals. *Acta Metall.* **34**, 1145 (1986).
- D. Yang and H. Conrad: Exploratory study into the effects of an electric field and high current density electropulsing on the plastic deformation of TiAl. *Intermetallics* **9**, 943 (2001).
- K. Okazaki, K. Kagawa, and H. Conrad: An evaluation of the contribution of skin, pinch and heating effects to the electroplastic effects in titanium. *Mater. Sci. Eng., A* **45**, 109 (1980).
- J.R. Lloyd: Electromigration in integrated circuit conductors. *J. Phys. D: Appl. Phys.* **32**, R109 (1999).
- R.P. Gupta, Y. Serruys, G. Brebec, and Y. Adda: Calculation of the effective valence for electromigration in niobium. *Phys. Rev. B* **2**, 669 (1983).
- Z.H. Xu, G.Y. Tang, F. Ding, S.Q. Tian, and H.Y. Tian: The effect of multiple pulse treatment on the recrystallization behavior of M3Al-1Zn alloy strip. *Appl. Phys. A* **88**, 429 (2007).
- S.H. Xiao, J.D. Guo, S.D. Wu, G.H. He, and S.X. Li: Recrystallization in fatigue copper single crystals under electropulsing. *Scr. Mater.* **46**, 1 (2002).
- Y.B. Jiang, G.Y. Tang, C.H. Shek, Y.H. Zhu, L. Guan, S.N. Wang, and Z.H. Xu: The effect of electropulsing treatment on the solid solution behavior of aged AZ61 alloy strip. *J. Mater. Res.* **23**, 2685 (2008).
- Y. Onodera and K.I. Hirano: The effect of direct electric current on precipitation in a bulk Al-4% Cu alloy. *J. Mater. Sci.* **11**, 809 (1976).
- H. Conrad: Effects of electric current on solid-state phase transformations in metals. *Mater. Sci. Eng., A* **287**, 227 (2000).
- W. Zhang, M.L. Sui, Y.Z. Zhou, and D.X. Li: Evolution of microstructures in materials induced by electropulsing. *Micron* **34**, 189 (2003).
- Y.Z. Zhou, J.D. Guo, W. Zhang, and G.H. He: Influence of electropulsing on nucleation during phase transformation. *J. Mater. Res.* **17**, 3012 (2002).
- Y.H. Zhu, S. To, W.B. Lee, X.M. Liu, Y.B. Jiang, and G.Y. Tang: Effects of dynamic electropulsing on microstructure and elongation of a Zn-Al alloy. *Mater. Sci. Eng., A* **501**, 125 (2009).
- S. To, Y.H. Zhu, W.B. Lee, X.M. Liu, Y.B. Jiang, and G.Y. Tang: Effects of current density on electropulsing induced phase transformation in a Zn-Al based alloy. *Appl. Phys. A* (in press).
- H. Conrad and A.F. Sprecher: *Dislocation in Solids* (Elsevier, Amsterdam, The Netherlands, 1989).
- P. Gumbsch and H.J. Gao: Dislocations faster than the speed of sound. *Science* **283**, 965 (1998).
- L. Xiao and H.C. Gu: Dislocation structures in zirconium and zircaloy-4 fatigued at different temperatures. *Metall. Mater. Trans. A* **28**, 1021 (1997).
- H. Conrad, J. White, W.D. Cao, X.P. Lu, and A.F. Sprecher: Effect of electric current pulses on fatigue characteristics of polycrystalline copper. *Mater. Sci. Eng., A* **145**, 1 (1991).
- Y.Z. Zhou, S.R. Qin, S.H. Xiao, G.H. He, and B.L. Zhou: Reversing effect of electropulsing on damage of 1045 steel. *J. Mater. Res.* **15**, 1056 (2000).
- Z.S. Xu, Z.H. Lai, and Y.X. Chen: Effect of electric current on the recrystallization behavior of cold worked α -Ti. *Scr. Metall.* **22**, 187 (1988).
- F. Ding, G.Y. Tang, Z.H. Xu, and S.Q. Tian: A new method for improving strength and plasticity of steel wire. *J. Mar. Sci. Technol.* **23**, 160 (2007).
- R.S. Qin and B.L. Zhou: Effect of electric current pulses on grain size in castings. *Int. J. Non Equilib. Process* **11**, 77 (1998).
- Y.H. Zhu and S. Murphy: General rule of decomposition reaction in supersaturated Zn-Al based alloy. *Chin. J. Metal Sci. Technol.* **2**, 1 (1986).
- Y.H. Zhu: General rule of phase decomposition in Zn-Al based alloys. II: On effect of external stress on phase transformation. *Mater. Trans., JIM* **45**, 3083 (2004).
- Y.H. Zhu: Microstructural changes in welded Zn-Al alloy. *J. Mater. Res.* **11**, 593 (1996).
- Y.H. Zhu, H.C. Man, H.C. Dorantes-Rosales, and W.B. Lee: Ageing characteristics of furnace cooled eutectoid Zn-Al based alloy. *J. Mater. Sci.* **38**, 2925 (2003).
- Y.H. Zhu and W.B. Lee: Tensile deformation and phase transformation of furnace cooled Zn-Al alloy. *Mater. Sci. Eng., A* **293**, 95 (2000).
- Y.H. Zhu and E. Orozco: Effects of tensile stress on microstructural change of eutectoid Zn-Al alloy. *Metall. Mater. Trans. A* **26**, 2611 (1995).
- Y.H. Zhu and J. Torres: Tensile deformation in extruded eutectoid Zn-Al based alloy. *Zeit Metall.* **88**, 392 (1997).
- Y.H. Zhu, W.B. Lee, and S. To: Tensile stress induced phase transformation of cast alloy ZnAl₇Cu₃. *Mater. Res. Bull.* **38**, 1851 (2003).
- Y.H. Zhu, W.B. Lee, C.Y. Chung, and S. To: On nanophase stability in eutectoid Zn-Al based alloy films. *Appl. Surf. Sci.* **236**, 106 (2004).